Materials Science, Vol. 21, No. 1, 2003

Magnetism of nanocrystalline and bulk $Fe_xNi_{23-x}B_6$ (x = 0, 1, 22 and 23) alloys – experiment and theory

B. IDZIKOWSKI*, A. SZAJEK

Institute of Molecular Physics, Polish Academy of Sciences,
M. Smoluchowskiego 17, 60-179 Poznań, Poland

Formation of the nanostructure composed of a metastable magnetically ordered *fcc*-$Fe_xNi_{23-x}B_6$ phase with large lattice constant (a = 1.051–1.082 nm) from amorphous $Fe_{81-y-z}Ni_yZr_7B_{12}Au_y$ (y = 10–40, 64; z = 0, 1) precursors due to the thermal treatment has been studied. Annealing of the $y \geq 20$, $z = 0$ samples at temperatures of 420–580 °C leads to an increase of $Fe_xNi_{23-x}B_6$ fraction embedded in amorphous matrix with grain sizes from a few to tens of nanometres. The structure transformations have been investigated by the DSC, XRD and TEM techniques. Magnetic behaviour of $Fe_xNi_{23-x}B_6$ (x = 0, 1, 22 and 23) phases has been studied theoretically using the spin polarized tight binding linear muffin-tin orbital (TB-LMTO) method. Anomalously high magnetic moments of Fe atoms have been found in some non-equivalent positions in the crystal structure.

Key words: *amorphous alloys; nanocrystallization; density of states; local magnetic moments*

1. Introduction

Investigations of crystallization processes of amorphous precursors have attracted a lot of attention in recent years because some of them form nanocrystalline structure. Such a reduction of the grain sizes influences drastically the physical behaviour of materials. The search continues for new nanocrystalline alloys with improved magnetic and mechanical properties, convenient for technical applications. Up to now these alloys, produced by a partial crystallization of amorphous precursors, have exhibited a two- or more-phase structure with body-centred cubic (*bcc*) nanocrystalline grains dispersed in a residual amorphous matrix. All known soft magnetic nanocrystalline alloys consist of nanosized *bcc*-Fe(Si) [1], *bcc*-Fe [2] or *bcc*-(FeCo) [3] grains with 3–15 nm in diameter. During the devitrification processes, the amorphous part of alloys becomes inhomogeneous, showing significant gradients of compositions.

*Corresponding author, e-mail: Bogdan.Idzikowski@ifmpan.poznan.pl.

The crystallization of Ni-containing amorphous alloys was studied earlier (e.g., [4, 5]) but those alloys were unsuitable for the formation of nanocrystalline alloys. However, the nanocrystalline grains were found in rapidly heated amorphous $Fe_{15}Ni_{60}Si_{10}B_{15}$ and $Fe_{20}Ni_{55}Si_{10}B_{15}$ systems [5]. The only Ni-containing amorphous system, $Fe_{40}Ni_{38}Mo_4B_{18}$, in which the nanostructured phase was clearly formed, was studied by the XRD technique [6]. In this case, the presence of Mo atoms in the alloy plays crucial role in the process of nanostructure formation because of the grains growth blocking. Extremely fine nanocrystalline structure is expected if small additions of e.g., Cu or Au are present in the amorphous precursor. Recently, Nakamura et al. [7] reported on the crystallization of amorphous $Fe_{70}Nb_{10}B_{20}$ alloy – the final product is *fcc*-$Fe_{23}B_6$ phase with a large lattice parameter. The authors observed in this system the nanometer-sized metastable $Fe_{23}B_6$ precipitates in the amorphous matrix before creation of the equilibrium *bcc*-Fe and boride phases in final crystallization state [7].

We prepared nickel-rich amorphous alloys $Fe_{81-y-z}Ni_yZr_7B_{12}Au_y$ (y = 10–40, 64; z = 0, 1) in which the nanostructure can be formed, as usually, by a controlled annealing but the significant presence of Ni in this alloys results in the formation of a metastable *fcc*-phase containing both transition elements (Ni and/or Fe) and boron. Because obtaining a pure single phase $TM_{23}B_6$ (TM = Fe, Ni) compounds by standard methods is difficult, we have also performed theoretical study of their magnetic behaviour.

2. Experimental

Fully amorphous ribbons with the nominal compositions $Fe_{81-y-z}Ni_yZr_7B_{12}Au_y$ (y = 10–40, 64; z = 0, 1) were prepared by the single roller (40 cm in diameter) technique in Ar protective atmosphere. High-purity elements (minimum 3*N*) were used to make starting pre-alloys. Each ingot was turned over several times and melted in the induction furnace water cooled boat to assure homogeneity. Long ribbons obtained were 2–3 mm wide and 0.35–0.45 μm thick. The structure of the samples was characterized by X-ray diffraction (XRD) analysis in a Seifert diffractometer using Cu-Kα radiation. The crystallization behaviour of as-quenched ribbons was examined with differential scanning calorimetry using DSC 404 made by Netzsch. For the transmission electron microscopy (TEM) studies, the samples were prepared by argon ion milling using 10 keV ions. TEM investigations were done using a Philips CM20 microscope (TWIN configuration, accelerating voltage: 200 kV), equipped with a Noran Voyager EDS system with Ge (Li) detector.

3. Results of measurements

Structural changes of amorphous precursors induced by thermal treatment were characterized by the differential scanning calorimetry (DSC) and X-ray diffraction (XRD) measurements. DSC linear-heating curves of all Ni-rich alloys investigated

show two crystallization stages. Such behaviour is typical of amorphous alloys serving as the precursors for the formation of the nanocrystalline alloys [8]. The crystallization temperature of the first stage is in the range of 460–520 °C. DSC measurements (not shown here) were carried out with 20 K/min heating rate. For samples $y \leq 20$ the nanocrystalline phase, which precipitates around the first exothermic peak, is *bcc*-Fe. If $y > 20$, the nanocrystallization product is *fcc*-$(Fe,Ni)_{23}B_6$. A similar crystallization behaviour was observed by Nakamura et al. in $Fe_{70}Nb_{10}B_{20}$ alloys where the average lattice constant $a = 1.067$ nm for the $Fe_{23}B_6$ fraction was assumed [7]. This lattice parameter (as well as other properties [9]) could differ from the values of bulk alloy because of two reasons: (i) interface of small grains can influence local crystal structure, (ii) relative large atoms of such elements as Nb or Zr could be placed inside the grain.

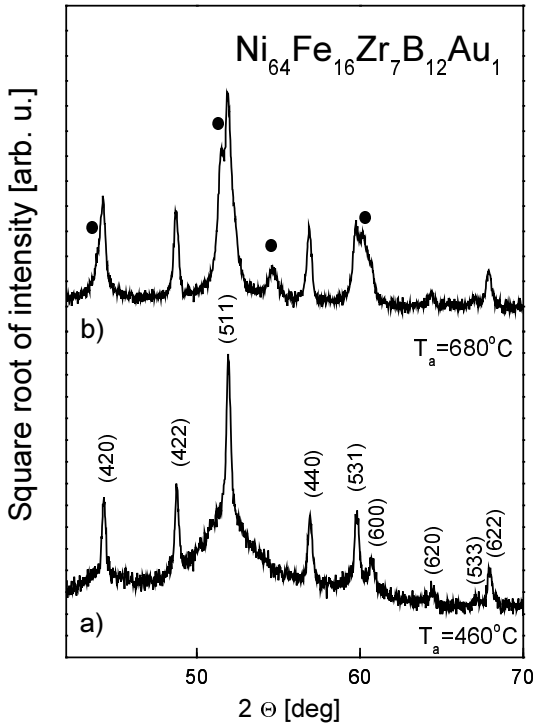

Fig. 1. X-ray diffraction (XRD) patterns for $Ni_{64}Fe_{16}Zr_7B_{12}Au_1$ ribbon after annealing at 460 °C and 680 °C for one hour

The as-quenched samples are fully amorphous, as found by XRD, with a broad diffuse peak around 43 degrees on 2Θ axis. Figures 1a and 1b show the structure of $Ni_{64}Fe_{16}Zr_7B_{12}Au_1$ partially crystallized after one-hour annealing at 460 °C and 680 °C, respectively. As a result of the annealing, grains of magnetically ordered cubic $Fe_xNi_{23-x}B_6$ phase appear in the amorphous matrix. All peaks have been identified

and all of them belong to the C_6Cr_{23}-type structure described by the space group $Fm(-3)m$. As shown in Fig. 1b, the increase of annealing temperature is connected with the decrease of the amount of the 23:6 phase, and the appearance of a new $(FeNi)_3B$ phase is marked by large black points.

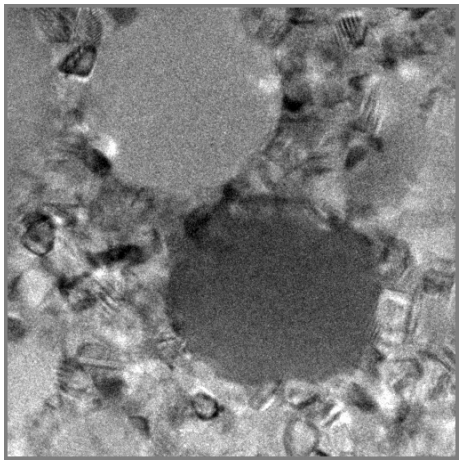

Fig. 2. Transmission electron micrograph of $Ni_{42}Fe_{40}Zr_7B_{12}$ alloy after annealing at 640 °C for one hour

TEM picture of $Ni_{42}Fe_{40}Zr_7B_{12}$ alloy heat treated at 640 °C is shown in Fig. 2. A fraction of very small grains (several nanometers in diameter) is present among relatively big grains. The chemical composition of small and big grains is the same, as has been confirmed by electron microdiffraction investigations (not shown here). The annealed nanocrystalline ribbons became magnetically soft because of exchange interaction between these small grains. A very similar mixture of majority small and minority big grains was found in HITPERM-type soft magnetic alloys.

4. Details of band structure calculations

The spin-polarized tight binding linear muffin-tin orbital (TB-LMTO) method in the atomic sphere approximation (ASA) [10, 11] was used to compute the electronic band structure of $Fe_{23}B_6$ and $Ni_{23}B_6$ compounds. In this approximation, the crystal is divided into space-filling spheres, therefore with slightly overlapping spheres centred on each of the atomic sites. The standard combined corrections for overlapping [10] were employed to compensate ASA errors. In the calculations reported here, the Wigner–Seitz (WS) sphere radii are such that the overlap is below 10%. The total volumes of all spheres S_j (j = 1, …, N) are equal to the volume (V) of the unit cell. The values of lattice constants of $Fe_{23-x}Ni_xB_6$, for x = 0, 1, 22 and 23, are extrapolated from the experimental data taken for x = 0 [12] and x = 4.5 [13] (see Fig. 3). The sys-

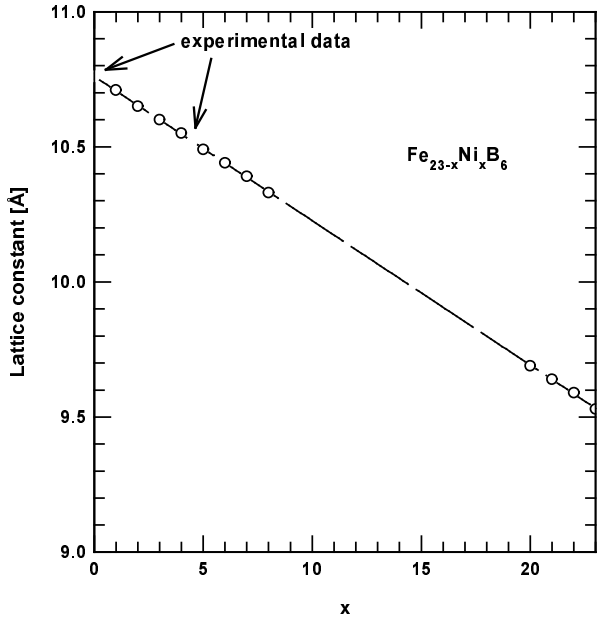

Fig. 3. Lattice constants for $Fe_{23-x}Ni_xB_6$ as a function of x.
Data for $x = 0$ and 4.5 are taken from the literature

Table 1. Structural parameters of $Fe_{23-x}Ni_xB_6$ compounds
(a = 1.0761, 1.071, 0.959 and 0.953 nm for x = 0, 1, 22 and 23) and *WS* radii S_j [Å]

Atom (position)	x	y	z	S_j			
				$x = 0$	$x = 1$	$x = 22$	$x = 23$
Fe or Ni (4a)	0	0	0	1.7007	1.6922	1.5177	1.5213
Fe or Ni (8c)	¼	¼	¼	1.5576	1.5498	1.3897 (1/2) 1.4040 (1/2)	1.3942
Fe or Ni (48h)	0	0.1699	0.1699	1.3852	1.3788	1.2286 (1/2) 1.2429 (1/4) 1.2286 (1/4)	1.2205
Fe or Ni (32f)	0.3809	0.3809	0.3809	1.3543	1.3480	1.2152(Ni; 1/8) 1.2152(Fe; 1/8) 1.2009(Ni; 3/8) 1.2009 (Ni; 3/8)	1.1930
B (24e)	0.2765	0	0	1.1908	1.1847	1.0615 (1/2) 1.0758 (1/2)	1.0683

tem has a cubic symmetry (for x = 0 and 23: $Fm(-3)m$ space group, No. 225). Its unit cells accommodate four formula units with N = 116 atoms. There are four non-equivalent positions of Fe(Ni) atoms (see Table 1) in the $Ni_{23}B_6$ and $Fe_{23}B_6$ compounds. The single atom impurities (Ni or Fe for x = 1 and 22, respectively) in

$Fe_{23-x}Ni_xB_6$ were located one after another in 4a, 8c, 48h, and 32f positions. The broken symmetry gives additional non-equivalent positions within 8c, 48h, 32f, and 24e sites for $x = 22$. They are presented in Table 1 for $x = 22$ together with their occupancy (in parentheses) within particular sites.

As starting, the following atomic configurations were assumed: core [Ar] + $3d^6 4s^2$ for Fe, core [He] + $2p^2 2s$ for B, and core [Ar] + $3d^8 4s^2$ for Ni. The fully relativistic approach for the core electrons and scalar relativistic approximation for the valence electrons were used. The Min–Jang [14] scheme for calculating the spin-orbit effects was employed. The exchange-correlation potential was chosen in the form proposed by von Barth–Hedin [15]. Self-consistent calculations were performed for 8000 *k*-points in the Brillouin zone. The tetrahedron method [16] was used for integration over the Brillouin zone. The iterations were repeated until the accuracy of the energy eigenvalues within the error of 0.01 mRyd was achieved.

5. Results of calculations

The TB LMTO ASA method allows differentation of the ions in the cell but the effect of disorder caused by Ni or Fe substitution is neglected. In the case of the C_6Cr_{23}-

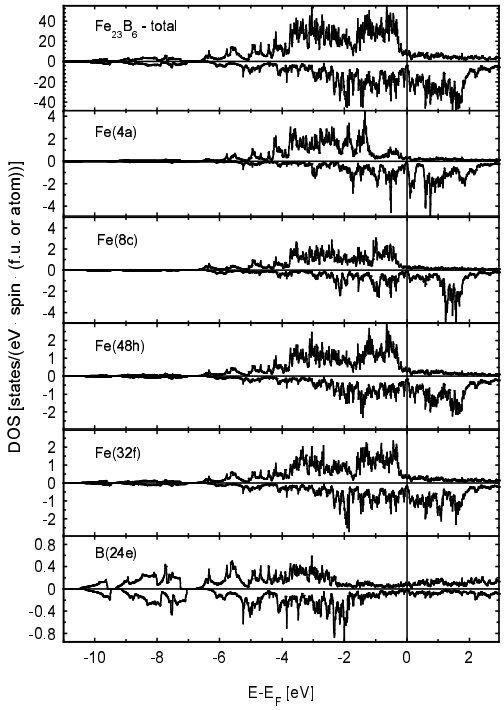

Fig. 4. Total and local density of states (DOS) plots for $Fe_{23}B_6$ compound

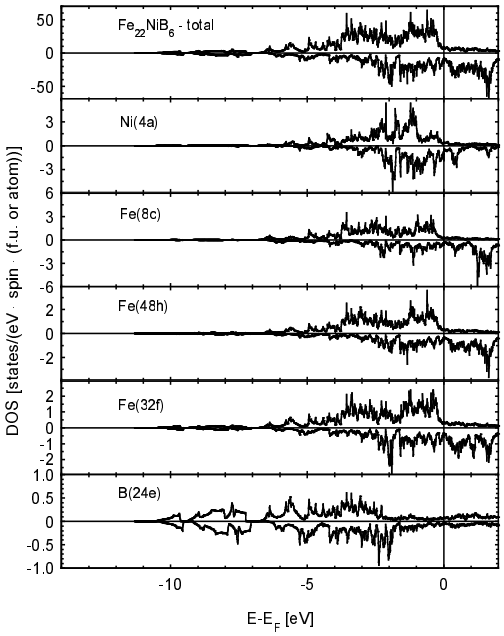

Fig. 5. Total and local density of states (DOS) plots for $Fe_{22}NiB_6$ compound

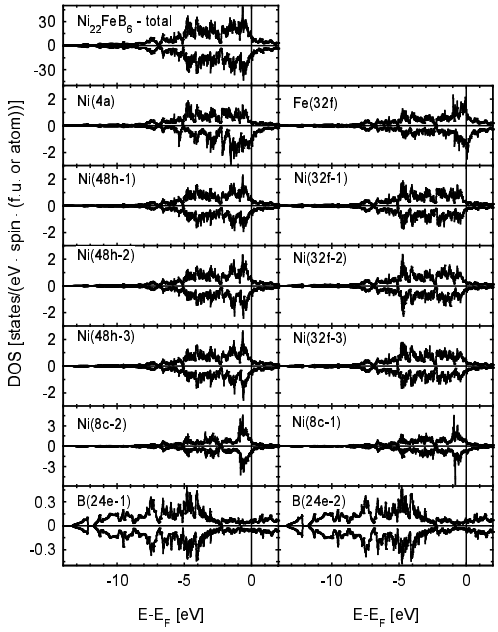

Fig. 6. Total and local density of states (DOS) plots for $Ni_{22}FeB_6$ compound

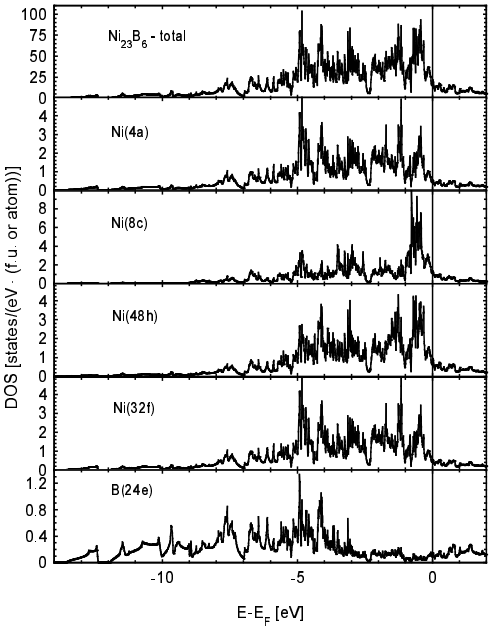

Fig. 7. Total and local density of states (DOS) plots for $Ni_{23}B_6$ compound

type structure the 4a, 8c, 48h, and 32f positions for Fe/Ni atoms have to be considered. Our total energy calculations show that in the case of $Fe_{22}NiB_6$ the Ni atoms prefer 4a position and in the case of $Ni_{22}FeB_6$ the Fe atoms prefer 32f sites. The results presented below concern the most stable localizations of the impurities, which minimize total energy. The total and local densities of states (DOS) for $Fe_{23-x}Ni_xB_6$ are presented in Figs. 4–7.

The shape of DOS plots depends on the type of the atom, its localization and local environment. The values of total DOS at the Fermi level (EF) are equal to 10.589, 25.184, 20.705 and 17.502 states/(eV f.u.) for x = 0, 1, 22 and 23, respectively. Because of a large number of d electrons that type of electrons provides the main contribution to the total DOS for E = E_F: about 90%. The exact values of site and l-decomposed spin-projected DOS at the Fermi level are collected in Table 2.

The calculated total magnetic moments for $Fe_{23}B_6$ and $Ni_{23}B_6$ compounds are equal to 48.758 and 0.742 μ_B/f.u. Local contributions provided by particular atoms are collected in Table 3.

Particularly high values of magnetic moments, for $Fe_{23}B_6$, are located on Fe(4a) and Fe(8c) atoms, higher than for the bulk *bcc*-Fe system (about 2.2 μ_B/atom). The values of magnetic moments depend on the local environment of Fe atoms. Increasing number of the neighbouring boron atoms reduces the magnetic moment of iron. In the case of $Ni_{23}B_6$ compound, the magnetic moments are reduced almost to zero, below 3×10^{-4} μ_B/atom.

Table 2. DOS at the Fermi level (states/(eV spin (atom or f.u.)))
of $Fe_{23-x}Ni_xB_6$ compounds (x = 0, 1, 22 and 23)

Atom (position)	Site and spin projected DOS (per atom)		Type of DOS	Total and l-decomposed spin projected DOS (per f.u.)	
	spin ↑	spin ↓		spin ↑	spin ↓
$Fe_{23}B_6$:			Total	6.577	4.012
Fe (4a)	0.227	0.140			
Fe (8c)	0.239	0.104	Total for:		
Fe (48h)	0.270	0.176	s electrons	0.310	0.030
Fe (32f)	0.281	0.182	p electrons	0.923	0.147
B (24e)	0.064	0.016	d electrons	5.344	3.835
$Fe_{22}NiB_6$:			Total	8.744	11.920
Ni (4a)	0.377	1.182			
Fe (8c)	0.308	0.534	Total for:		
Fe (48h)	0.363	0.477	s electrons	0.369	0.087
Fe (32f)	0.366	0.455	p electrons	1.074	0.742
B (24e)	0.079	0.051	d electrons	7.298	11.099
$Ni_{22}FeB_6$:			Total	9.570	11.135
Ni (4a)	0.245	0.997			
Ni (8c-1)	0.648	0.652	Total for:		
Ni (8c-2)	0.603	0.785	s electrons	0.240	0.226
Ni (48h-1)	0.394	0.410	p electrons	0.724	0.681
Ni (48h-2)	0.398	0.476	d electrons	8.606	10.228
Ni (48h-3)	0.389	0.407			
Ni (32f-1)	0.244	0.239			
Ni (32f-2)	0.251	0.266			
Ni (32f-3)	0.301	0.355			
Fe (32f)	1.091	1.211			
B (24e-1)	0.059	0.050			
B (24e-2)	0.060	0.043			
$Ni_{23}B_6$:			Total	8.751	8.751
Ni (4a)	0.253	0.253			
Ni (8c)	0.646	0.646	Total for:		
Ni (48h)	0.400	0.400	s electrons	0.228	0.228
Ni (32f)	0.253	0.253	p electrons	0.906	0.906
B (24e)	0.064	0.064	d electrons	7.617	7.617

Table 3. Local magnetic moments for Fe, Ni, and B atoms in $Fe_{23-x}Ni_xB_6$ compounds (x = 0, 1, 22 and 23)

Compound	Magnetic moments [μ_B/atom] for given position				
	4a	8c	48h	32f	24e
$Fe_{23}B_6$	2.982	2.553	2.222	1.877	–0.167
$Fe_{22}NiB_6$	0.719(Ni)	2.512 (Fe)	2.198 (Fe)	1.829 (Fe)	–0.168
$Ni_{22}FeB_6$	0.140	0.186 (1/2) 0.077 (1/2)	0.053 (1/2) 0.044 (1/4) 0.032 (1/4)	0.008 (Ni; 1/8) 0.575 (Fe: 1/8) 0.024 (Ni; 3/8) 0.045 (Ni; 3/8)	–0.010 (1/2) –0.002 (1/2)
$Ni_{23}B_6$	0.000	0.000	0.000	0.000	0.000

6. Conclusions

Band structure calculations showed that the local magnetic moments of Fe and Ni atoms in $Fe_{23}B_6$ and $Ni_{23}B_6$ compounds depend on their local environments. The iron magnetic moments are enhanced up to about 3 μB/atom, being reduced for nickel, even to zero. Calculations of the total energy show that in $Fe_{22}NiB_6$ the Ni atoms are located in the 4a position and in $Ni_{22}FeB_6$ the Fe atoms preferably locate at 32f sites. The investigations presented in this contribution will be continued for all x substitutions in $(Fe_{1-x}Ni_x)_{23}B_6$ systems to determine the dependence of magnetization on concentration of Ni impurities and their site preference.

In the nanocrystalline state, Ni-rich alloys show good mechanical properties compared with the FINEMET, NANOPERM or HITPERM. The improved magnetic properties and reduced brittleness of the samples offer attractive possibilities for applications of this alloy. It is of particular interest to study such alloys and to attempt understanding details of the complex crystallization process leading to the formation of new *fcc*-based soft magnetic nanostructured alloys.

Acknowledgements

The authors thank M. Giersig from Hahn Meitner Institute Berlin, Germany, for performing the TEM investigations.

References

[1] YOSHIZAWA Y., OGUMA S., YAMAUCHI K., J. Appl. Phys., 64 (1988), 6044.
[2] SUZUKI K., KTAOKA N., INOUE A., MAKINO A., MASUMOTO T., Mat. Trans. JIM, 31 (1990), 743.
[3] WILLARD M.A., LAUGHLIN D.E., MCHENRY M.E., THOMA D., SICKAFUS K., CROSS J.O., HARRIS V.G., J. Appl. Phys., 84 (1998), 6773.
[4] HERZER G., Phys. Scr., T49 (1993), 307.
[5] MIZGALSKI K.P., INAL O.T., YOST F.G., KARNOWSKY M.M., J. Mater. Sci., 16 (1981), 3357.
[6] LI J., SU Z., WANG T.M, GE S.H., HAHN H., SHIARI Y., J. Mater. Sci., 34 (1999), 111.

[7] NAKAMURA T., KOSHIBA H., IMAFUKU M., INOUE A., MATSUBARA E., Mater. Trans., 43 (2002), 1918.
[8] KONDORO J.W., CAMPBELL S.J., Hyperfine Inter., 55 (1990), 993.
[9] ŚLAWSKA-WANIEWSKA A., GRENECHE J.M., Phys. Rev., B56 (1997), R8491.
[10] ANDERSEN O.K., JEPSEN O., ŠOB M., *Electronic Structure and its Applications*, M.Yussouff (Ed.), Springer, Berlin (1987), p. 2.
[11] KRIER G., JEPSEN O., BURKHARDT ANDERSEN O.K., *The TB-LMTO-ASA Program (source code, version 4.7)*.
[12] KHAN Y., WIBBEKE H., Z. Metalkd., 82 (1991), 703.
[13] AYEL M., RIVIERE R., MONNIER G., Compt. Rend., 264C (1967), 862.
[14] MIN B.I., JANG Y.-R., J. Phys.: Condens. Matter, 3 (1991), 5131.
[15] BARTH U., HEDIN L., J. Phys., C5 (1972), 1629.
[16] BLÖCHL P., JEPSEN O., ANDERSEN O.K., Phys. Rev., B49 (1994), 16223.

Received 4 December 2002
Revised 31 January 2003